ACS Chemical Neuroscience

Research Article

pubs.acs.org/chemneuro

Fluorescent Filter-Trap Assay for Amyloid Fibril Formation Kinetics in Complex Solutions

Irem Nasir,* Sara Linse, and Celia Cabaleiro-Lago

Department of Biochemistry and Structural Biology, Center for Molecular Protein Science, Lund University, P.O. Box 124, SE 221 00, Lund, Sweden

Supporting Information

ABSTRACT: Amyloid fibrils are the most distinct components of the plaques associated with various neurodegenerative diseases. Kinetic studies of amyloid fibril formation shed light on the microscopic mechanisms that underlie this process as well as the contributions of internal and external factors to the interplay between different mechanistic steps. Thioflavin T is a widely used noncovalent fluorescent probe for monitoring amyloid fibril formation; however, it may suffer from limitations due to the unspecific interactions between the dye and the additives. Here, we present the results of a filter-trap assay combined with the detection of fluorescently labeled amyloid β (Aβ) peptide. The filter-trap assay separates formed aggregates based on size, and the fluorescent label attached to Aβ allows for their detection. The times of half completion of the process ($t_{1/2}$) obtained by the filter-trap assay are comparable to values from the ThT assay. High concentrations of human serum albumin (HSA) and carboxyl-modified polystyrene nanoparticles lead to an elevated ThT signal, masking a possible fibril formation event. The filter-trap assay allows fibril formation to be studied in the presence of those substances and shows that Aβ fibril formation is kinetically inhibited by HSA and that the amount of fibrils formed are reduced. In contrast, nanoparticles exhibit a dual-behavior governed by their concentration.

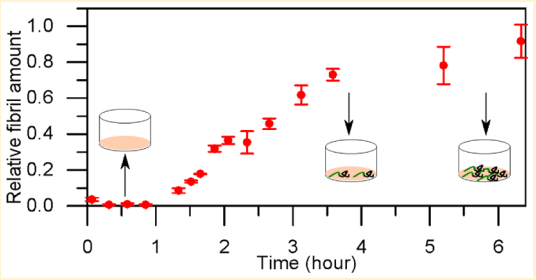

KEYWORDS: *Amyloid, aggregation, kinetics, filter-trap, site-specific fluorophore labeling, Alzheimer's disease*

Alzheimer's disease (AD) is a fatal neurodegenerative disease and the most common form of dementia. The absolute cause remains unknown, and there is no therapeutics that can stop the progression of the disease.[1] The characteristic hallmark of the disease in the human brain is extracellular amyloid plaques that consist of fibrillar aggregates of a natively unfolded peptide, amyloid beta (Aβ), which commonly exists as 40 and 42 residue isoforms.[2−5] Amyloid fibrils have a common architecture of extended β sheets, in which β strands of Aβ monomers run perpendicular to the fibril axis. According to the amyloid cascade hypothesis, Aβ is a main actor in the development of the AD by forming oligomers and fibrils consecutively leading to the deposition of plaques.[6]

Kinetic studies of the fibril formation of amyloid peptides *in vitro* have provided insight into the mechanism of the process. Kinetic data have been used to determine the underlying microscopic mechanisms of fibrillation of several amyloidogenic peptides and to investigate the influence of sequence mutations on the aggregation propensity of diverse proteins.[7,8] Moreover, the effect of putative antiamyloid compounds, including peptides and proteins, polymers, small organic compounds, or nanoparticles on the fibril formation process has been studied[9−16] and has provided valuable information about the mechanisms of inhibition and of the development of potential therapeutics.

Dye binding assays are by far the most used methods to quantify amyloid fibril formation. Noncovalent amyloid-specific dyes, such as Thioflavin T (ThT) and Congo red, are widely used for this purpose. ThT is a benzothiazole dye that fluoresces when bound to extended β sheets and possesses weak fluorescence in the absence of these structures.[17] Hence, the increase in fluorescence intensity correlates with fibril formation, and detection over a time period reveals the fibrillation kinetics of amyloidogenic peptides. There are two common ways to follow the kinetics of fibril formation with ThT: a continuous assay, where ThT is present from the beginning of the fibril formation process, and a noncontinuous assay where individual samples are taken during the fibril formation and diluted with ThT-containing buffer. Alongside the *in vitro* kinetic assays, amyloid fibril formation must be verified by other techniques. Existence of fibrils as well as fibrillar morphologies can be monitored by using atomic force microscopy (AFM) or transmission electron microscopy (TEM).[18]

The ThT assay is considered the gold standard among the dye binding assays that are used for amyloid fibril formation as the signal outcome is highly reproducible if the experimental conditions are optimized.[19] Furthermore, while binding to the

Received: April 2, 2015
Published: May 6, 2015

DOI: 10.1021/acschemneuro.5b00104
ACS Chem. Neurosci. 2015, 6, 1436−1444

species at one side of the equilibrium might disturb the equilibrium through thermodynamic linkage, reliable kinetic parameters of amyloid fibril formation can still be obtained. This is most likely due to a high association rate of the dye to fibrils after they have formed and the fact that the back-reaction is too slow for any perturbation by the dye to affect the observed association kinetics. The ThT signal can be biased by the presence of exogenous compounds. These compounds can interact with free ThT in solution increasing the fluorescence intensity in a manner similar to that of amyloid aggregates. In this situation, the high initial fluorescence signal masks the fibril formation signal and precludes fitting with functions that represent the time dependent evolution of the process. Furthermore, diverse substances[20−22] have been reported to interfere with the ThT assay, either by quenching the fluorescence or by affecting the binding of ThT to amyloid structures.

Filter-trap assays provide an alternative to dye binding assays. In short, samples are filtered through a membrane, and the material trapped on the membrane is quantified. These assays have been used previously for the detection and quantification of amyloid aggregates formed by diverse proteins. In general, the retained aggregates have been quantified by antibodies.[23−25] Drawbacks of such an immunodetection approach are its time consumption, sensitivity to the quality of the antibodies, required optimization steps of concentrations of primary and secondary antibodies, and lack of a linear correlation between signal and concentration in a wide range, which hampers the quantification. Furthermore, it requires harsh washing conditions, which possibly can impair the integrity of the structures deposited on the membrane. Another detection method used is radiolabeling of the amyloid protein, which provides high sensitivity, but is a laborious and costly process. Fluorophore-labeling has been used combined with a filter retardation assay to determine the effect of certain chemical compounds on the aggregation of HET-s protein; however, the study provided no time resolution of fibril formation.[26] We present here a novel approach to use the filter-trap assay combined with fluorophore labeling for the determination of amyloid fibril formation kinetics.

In this study, we describe the filter-trap method as an alternative to conventional dye binding assays to study amyloid fibril formation kinetics. The present work fills the gap of a simple and high-throughput assay that resolves the stages of fibril formation when the common methods are deficient for technical reasons. Briefly, the method is based on labeling the monomers with a fluorophore and filtering the on pathway aggregates on a membrane plate that has a certain size cut off. Retained and flowed through materials are quantified by using the advantage of the covalently linked fluorophore label. The results demonstrate that the method successfully resolves all stages of the fibril formation process as good as the ThT assay in a semicontinuous manner. As a suitable application of the method, the fibril formation process was monitored for Aβ42 by the filter-trap assay in the presence of two ThT-interfering substances: human serum albumin (HSA) and carboxyl-modified negatively charged polystyrene nanoparticles.

RESULTS AND DISCUSSION

In the present study, a membrane filter-trap assay was developed for following *in vitro* amyloid fibril formation kinetics for cases when dye binding assays are inadequate. It is a high-throughput and simple method, based on fractionating the components according to their size, therefore in most cases interference caused by additives is eliminated. Here, we have based our approach on collecting time-point samples during the fibril formation time course and filtering through a 96-well membrane plate of a desired cut off size. The filter-membrane traps amyloid aggregates above a defined size (here, a 0.2 μm cut off was used), whereas smaller aggregates and monomers that pass through are collected in a regular 96-well plate as seen in Figure 1. The detection of fibrillar aggregates as well as smaller aggregates or monomers that pass through is performed on two different plates, where the fibrillar material and flow through are collected separately, and relies on site-specific, covalent labeling of Aβ42 monomer at a single position (via an N-terminal cysteine) with a fluorescent dye. Consequently, the amyloid fibril formation process can be followed by quantification of the fluorescence intensity of the label on the filter membrane and in the flow through.

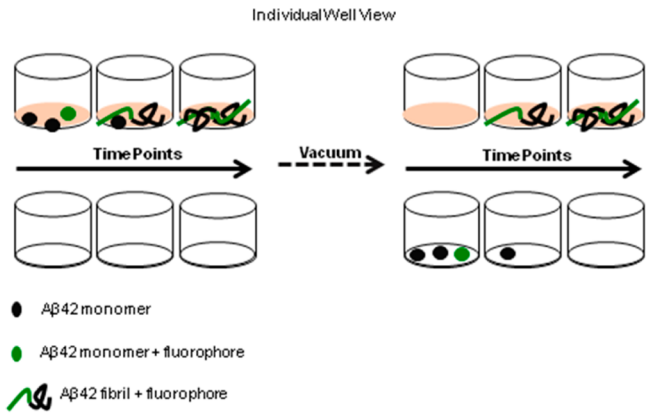

Figure 1. Illustration of the principle behind the method. Top row of sample wells represent the GHP membrane plate, where the retentate is collected, and the bottom row of sample wells represent the transparent bottom plate, where the flow-through is collected.

Technical Considerations. The basis of the filter-trap assay relies on three important factors: the selection of a fluorophore that is covalently linked to the monomers, the design of a peptide with a specific labeling site, and the selection of a proper membrane plate that separates and retains the fibrillar aggregates in a non-invasive way.

In this study, we used two different dyes, Alexa Fluor 488 dye and IRDye 680RD infrared dye, as candidates to label the Aβ42 monomer separately. IRDye 680RD infrared dye has an advantage of higher sample to blank ratio than Alexa Fluor 488 dye, due to low contribution of the plate housing to the fluorescence signal in the near-infrared region of the spectrum. Using amine-reactive dyes brings with it the risk of labeling the peptide disproportionally because of the two Lys residues and an N-terminal amine group of the Aβ42 peptide. As a consequence, a peptide can be labeled more than one time which reduces the homogeneity of the sample. Moreover, the risk of interference with aggregation appears because of labeling Lys residues which are in the β-sheet forming region of Aβ. Maleimide chemistry requires thiol groups, which are absent in the native sequence. Redesigning the Aβ42 peptide to bear a Cys residue allowed us to efficiently label the peptide (see Table S1, Supporting Information, for the comparison of the native and redesigned sequences). It is very crucial to select the location of the dye because the kinetics of fibril formation are

DOI: 10.1021/acschemneuro.5b00104
ACS Chem. Neurosci. 2015, 6, 1436−1444

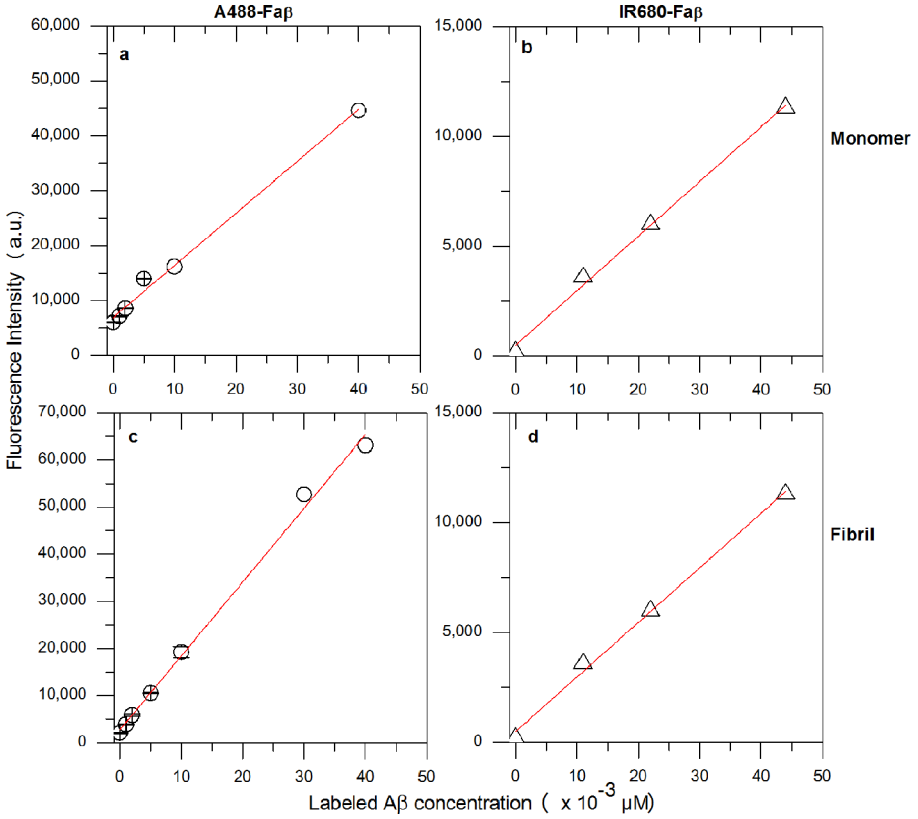

Figure 2. Linear dependence of fluorophore intensity on labeled Aβ within FAβ42. Each point represents the average of 2 or 3 replicates, and the error bars represent the standard deviation. Top row: fluorophore intensity correlation with labeled Aβ concentration measured in a black polystyrene plate with a clear bottom. (a) Alexa Fluor 488 dye; (b) IRDye 680RD infrared dye. Bottom row: Fluorophore intensity correlation with labeled Aβ concentration trapped as fibrils and measured on a GHP membrane. (c) Alexa Fluor 488 dye; (d) IRDye 680RD infrared dye.

sensitive to the modifications within the peptide sequence; thus, labeling the peptide can potentially affect the fibril formation kinetics as well as the structure of the fibrils formed.[27] Aβ peptide has a β-sheet forming core starting from residue number 16 and extending to the C-terminus;[28] thus, inserting a dye of a size comparable to five amino acids at the center or C-terminus sites may affect fibril formation. Additionally, the N-terminus of the Aβ peptide is rather flexible compared to that of the other regions of the peptide mentioned previously, suggesting the idea of the N-terminus being the most suitable site to label. Accordingly, the Aβ42 peptide was designed to bear a cysteine at the N-terminus (Aβ(MC1−42)) where the fluorophore is covalently linked using maleimide chemisty. The degree of labeling, which is the ratio of incorporated label to the total concentration of monomeric peptide, was between 3% and 6% for both dyes. Because of the high quantum yield of the labels, we have used a mix of labeled and unlabeled Aβ42 peptide, which henceforth will be referred to as A488-FAβ42 or IR680-FAβ42 for Alexa Fluor 488 dye and IRDye 680RD infrared dye, respectively.

Using a multiwell platform allows the kinetics of amyloid fibril formation to be studied in many different conditions with several replicates simultaneously. The filter-trap assay is based on filtering the individual samples and measuring the amount of fibrils formed for each individual sample at a certain time-point through the reaction. Therefore, the collection of individual samples with replicates at different time points throughout the fibril formation allows us to reconstruct an amyloid fibril formation kinetic trace with the characteristic sigmoidal-like profile. Single point detections at the end point of fibril formation do not provide detailed information about the effect of additives to the amyloid fibril formation process. For example, the same levels of fibrils can be observed in an end point assay for a fibril formation process that is only kinetically inhibited (slower lag and growth phases but the same plateau levels).[22] A "semi-continuous" method as the one described here provides more information on the process such as the variations of $t_{1/2}$, fibril growth rates, the amount of fibrils formed, and the entire curve shape, which are necessary for a mechanistic understanding of the role of inhibitors.[29] We have assessed many different filter membrane plates with various membrane and housing materials. As described above, the basis of the method relies on fluorescence detection requiring a low protein binding membrane with high sample to blank ratio to be able to detect the smallest changes of the fluorophore intensity, which is attributed to the amyloid fibril formation. Filter plates of different membranes such as hydrophilic polypropylene (hereafter referred as GHP), polyPVDF, Durapore, mixed cellulose, BioTrace NT, Bio-Inert, Supor PES, and glass fiber were tested. In most cases, the autofluorescence of the membrane was found to hinder their use. A comparison of sample to blank ratio for three different plates is shown in Supporting Information, Table S2. Among the plates tested, only the GHP membrane plate gave a significant sample to blank ratio (the highest for given fluorophore concentration) when fibrils are deposited on the membrane.

Fluorescence Signal of Labels Correlates Linearly with the Concentration of Monomers and Fibrils. A prerequisite for a quantitative use of this method is a linear

DOI: 10.1021/acschemneuro.5b00104
ACS Chem. Neurosci. 2015, 6, 1436−1444

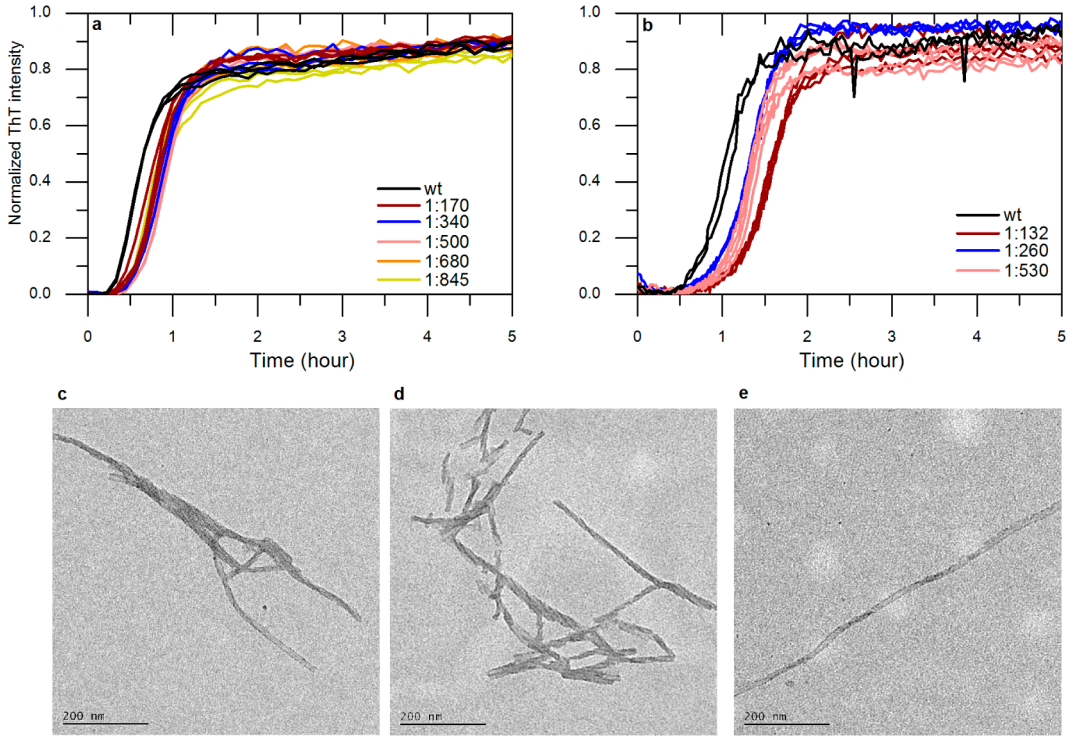

Figure 3. Effect of the fluorophore label on fibril formation kinetics and morphology of Aβ42. Top row: ThT fibrillation traces of (a) wild type Aβ42 and A488-FAβ42, and (b) wild type Aβ42 and IR680-FAβ in a given ratio of [dye]/[wt Aβ42 monomer]. Total starting monomer concentrations are 5 μM and 4 μM, respectively. Bottom row: TEM images of fibrils of (c) wild type Aβ42, (d) A488-FAβ42, and (e) IR680-FAβ42. Monomer concentrations of (d–f) are 2.5 μM, 4 μM, and 3 μM, respectively. The scale bar represents 200 nm.

correlation between the fluorescence intensity of the labeled peptide and the concentration of monomer and fibril bound fluorophores, within the concentrations range used in the experiments. Figure 2 shows the relationship between the fluorescence signals of A488-FAβ42 and IR680-FAβ42 to the concentration. The correlation of fluorescence intensity with labeled monomeric peptide concentration is linear in a broad concentration range for A488-FAβ42 or IR680-FAβ42 as seen in Figure 2a and b. Furthermore, the signal of trapped material on GHP correlates also linearly with the concentration of labeled monomer used for the preparation of the fibrils as seen in Figure 2c and d, assuming that the ratio of labeled peptide to unlabeled peptide stays constant throughout the amyloid fibril formation. Note that the instrument gain is adjusted for the best signal-to-noise ratio depending on the measurement plate of the subject material, i.e., for monomers the 96-well black plate and for fibrils GHP membrane plate are used.

Labeling Does Not Significantly Affect the Fibrillation Kinetics of Aβ42. In order to rule out undesirable alterations due to the labeling of the monomer on the fibrillation kinetics, the fibrillation process of A488-FAβ42 or IR680-FAβ42 at different molar ratios of labeled to unlabeled peptide was followed by the ThT assay and compared to the fibril formation process of Aβ42 in the absence of the labeled peptide (Figure 3a and b). Slight delays on the kinetics of Aβ42 were observed due to the addition of labeled peptide regardless of the molar ratio of labeled peptide to unlabeled peptide in the studied range. These findings further support the low impact of mixing the unlabeled peptide with the labeled peptide.

Addition of a label may also influence the morphology of the fibrils formed.[30] TEM images indicate that there is no detectable difference in morphology between the fibrils of Aβ42 and FAβ42, in terms of twist and thickness of the fibrils, as seen in Figure 3c–e.

Filter-Trap Assay Half Times Are Comparable to Those Obtained by the ThT Assay. In order to evaluate the proposed method after the mentioned optimization steps, the ThT assay and filter-trap assays were run in parallel to the filter-trap assay. ThT intensity was measured continuously to guide the sampling of time points for the new method, until the apparent plateau intensity was reached. Samples with no ThT were collected at a series of time points and transferred to the GHP membrane plate and vacuum was applied. The fluorescence intensity of the label fluorophore was measured on the membrane surface and for the collected flow through.

As expected, the fluorescence intensity on the GHP membrane increases as the fibril formation proceeds. A short lag phase is followed by a growth phase, and finally, an equilibrium plateau is observed, as shown in Figure 4. The increase in fluorescence intensity indicates the accumulation of material that is bigger than the membrane size cutoff. Additionally, the fluorescence intensity in the flow through fraction decreases inversely with the increase of the retentate fluorescence intensity. The decrease in the intensity of the flow through reflects depletion of nonfibrillar material from the solution. From the kinetic traces of both the retentate and flow through fractions, the half time ($t_{1/2}$), the time required for half of the peptide to form fibrils, can be calculated. The $t_{1/2}$ values obtained from the retentate trace and the flow through trace are similar, demonstrating the complementarity of both kinetic traces and indicating that all of the components for mass balance are accounted for. Overall, the shape of fibril formation curves from the filter-trap assay reproduces the curves obtained by the ThT assay, which implies that the new method can

DOI: 10.1021/acschemneuro.5b00104
ACS Chem. Neurosci. 2015, 6, 1436–1444

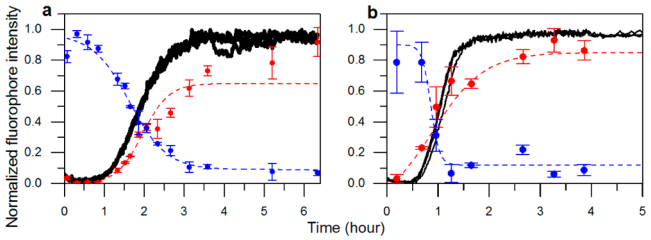

Figure 4. Filter-trap assay compared with the ThT assay. The continuous black line shows the ThT traces of the corresponding control. Red dots are normalized fluorescence intensities of FAβ42 on the GHP membrane, and blue dots are normalized intensities of FAβ42 in the transparent bottom plate. The dashed lines are a guide to the eye, and the error bars represent the standard deviation from three replicates performed. (a) Assay performed with A488-FAβ42 with a total starting monomer concentration of 2.5 μM. (b) Assay performed with IR680-FAβ42 with a total starting monomer concentration of 4 μM.

resolve all steps of the fibril formation as the ThT assay does. In general, the filter-trap assay reports a later onset of fibril formation to the ThT assay of an average of 18% of $t_{1/2}$. The kinetic traces obtained by the filter-trap assay compared to the traces obtained by the ThT assay confirm that the filter-trap assay is a suitable method to analyze the kinetics of amyloid fibril formation. Discrepancy between the two methods can arise because the filter-trap assay only detects aggregates larger than membrane cut off (200 nm), which readily possess many ThT binding units. Although fluorophores used in this study are more sensitive than ThT in terms of emission intensity per concentration, the formation of sufficiently large fibrils combined with the possibility of the loss of nonfibrillar material from the solution to flow through leads to a slower apparent growth rate compared to that in the ThT assay.

Given the dye to protein ratio and the assured linearity of the fluorescence signal, the peptide concentration trapped on the filter membrane and in the flow through can be calculated. The fluorescence signal from the flow through trace is compatible with a 15% concentration of the original monomer concentration (e.g., 85% fibrillar material is deposited on the filter membrane). However, 99% conversion of the monomer to fibrils has been reported in the literature.[31] This indicates that not only the monomer but also small oligomers or fragments of fibrils pass through the filter membrane as supported by the existence of fibrils in negative staining EM images of flow through fractions (Figure S1, Supporting Information). For that reason, the exact total amount of fibrillar material formed and trapped on the membrane cannot be determined; however, it is possible to estimate the relative increase or decrease of fibrillar material with respect to the FAβ42 control, when the effect of an additive on fibrillation is in question.

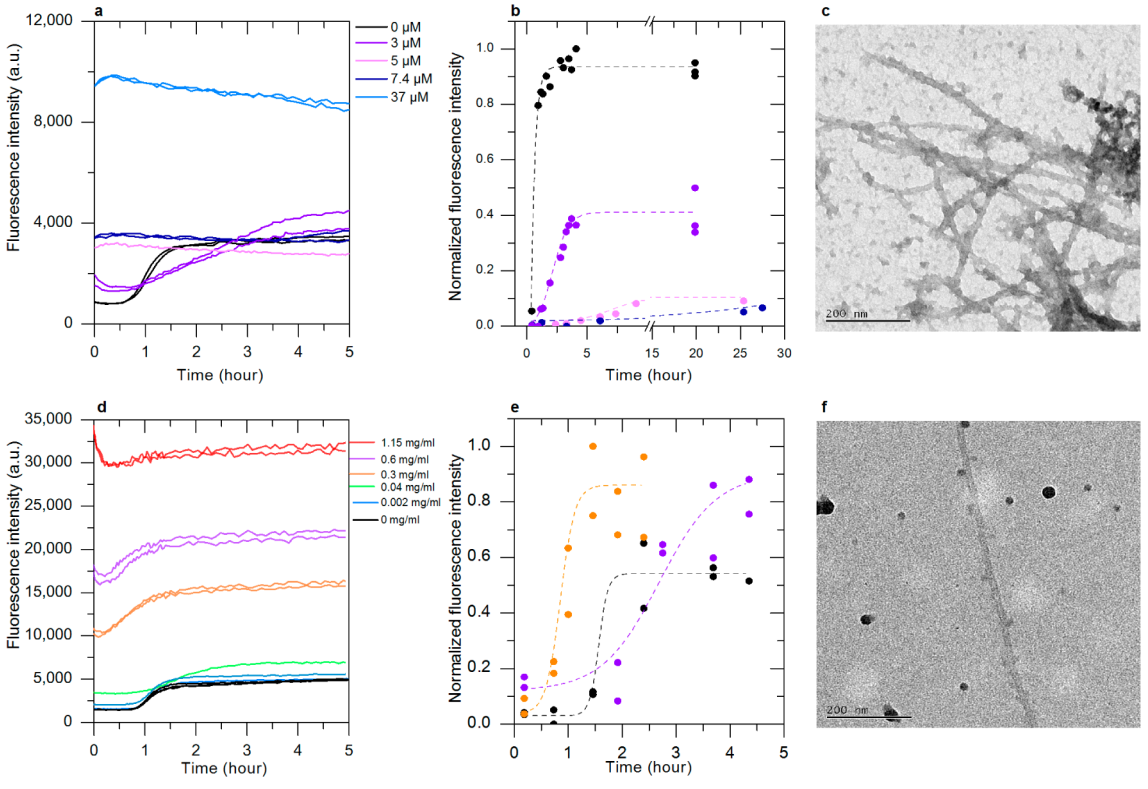

Figure 5. Application of the method. Top panels: effect of HSA on fibrillation kinetics of 4 μM A488-FAβ42 (ratio 1:500). (a) ThT traces of Aβ42 incubated with the indicated concentrations of HSA. (b) Filter-trap assay results for 0 μM (black), 3 μM (violet), 5 μM (pink), and 7.4 μM (navy) HSA of A488-FAβ42. The dashed lines are a guide to the eye. (c) Negative-staining EM image of A488-FAβ42 before the application of the filter-trap assay in the presence of 3 μM HSA. Bottom panels: Effect of 49 nm nominal size carboxyl modified polystyrene particles on the fibrillation kinetics of 3 μM IR680-FAβ42 (ratio 1:132). (d) ThT traces of Aβ42 incubated with the indicated concentrations of carboxyl modified polystyrene nanoparticles. (e) Filter-trap assay results for 0 mg/mL (black), 0.3 mg/mL (orange), and 0.6 mg/mL (violet) carboxyl modified polystyrene particles of IR680-FAβ42. The dashed lines are a guide to the eye. (f) Negative-staining EM image of IR680-FAβ42 before the filter-trap assay in the presence of 0.3 mg/mL carboxyl modified polystyrene particles. The scale bars represent 200 nm.

DOI: 10.1021/acschemneuro.5b00104
ACS Chem. Neurosci. 2015, 6, 1436−1444

Amyloid Fibrillation Kinetics of FAβ42 in the Presence of ThT-Interfering Substances Can Be Followed by the Filter-Trap Assay. After having established that the filter-trap assay reliably reports on the kinetics on FAβ42 fibril formation, we monitored the effect of additives on fibril formation. We picked HSA and carboxyl modified polystyrene nanoparticles as they interfere with the ThT assay above certain concentrations. Elevated ThT signal in the presence of those additives limits studying the effects of those substances on the fibrillation of Aβ42 in a wide range of concentrations.

HSA is the most abundant protein in blood plasma and plays a vital role in regulating the osmotic pressure. It also helps in transport, as HSA binds many other ligands in plasma,[32] which makes HSA a good candidate for model studies of protein−ligand interactions. Low levels of Aβ in blood plasma compared to that in cerebrospinal fluid (CSF) and the significantly higher HSA concentration in blood plasma compared to that in the CSF further suggest that binding and trapping of Aβ by HSA may be relevant.[33,34] However, serum albumins, with affinity for a multitude of large and small molecules, distort the ThT signal. Figure 5a shows the ThT traces of FAβ42 fibrillation at increasing HSA concentrations. ThT intensities are altered starting from 3 μM HSA onward, and higher HSA concentrations yield curves without the typical sigmoidal behavior. Furthermore, ThT intensity increases in HSA in a concentration dependent fashion. These findings are in line with a previously reported study by Khan and co-workers, where they have scrutinized the mechanism of ThT binding to the four most abundant serum albumin variants and found out that HSA has the highest affinity to ThT and that the intensity increased in a concentration dependent manner.[35] Figure 5b shows amyloid fibril formation monitored by the filter-trap assay at three concentrations of HSA, including those in which A488-FAβ42 fibril formation cannot be studied in the presence of HSA by the ThT assay. In the presence of HSA, the apparent elongation rate of A488-FAβ42 decreases with increasing concentration of HSA. The plateau values are also lowered compared to the control fibrillation of A488-FAβ42 in the absence of HSA, indicating that less fibrillar material is trapped on the membrane in the presence of HSA, suggesting that less fibrillar material is formed in this case. TEM images of aggregates formed in the presence of 3 μM HSA before filtering show fibrillar rather than amorphous aggregates (Figure 5c). This finding confirms that the lower amount of fibrillar material trapped is not explained by the formation of smaller aggregates that might have passed through the membrane leaving less fibrillar material trapped, but indeed suggests that less fibrillar material forms in the presence of HSA. The decoration along the amyloid fibrils in the TEM image is likely to come from the presence of HSA because images taken without HSA show no trace of this feature; furthermore, smaller fibrils have characteristic defined edges. The effect of increasing HSA concentration on the negative-staining images of A488-FAβ42 fibrils can be seen in Figure S2 (Supporting Information). Finally fibrillar material that is trapped on the membrane consists only of A488-FAβ42, as HSA does not aggregate in the experimental conditions used.[36]

The filter-trap assay data suggests that HSA delays fibril formation in a concentration-dependent manner. Moreover, the amount of fibrils retained on the GHP membrane plate decreases in the same manner. The effect can be explained by HSA trapping A488-FAβ42 oligomers, and therefore decreasing the effective concentration of monomers left in solution for fibrillation as proposed earlier by Milojevic et al.[37−39] Stanyon and Viles studied the kinetics of fibrillation of Aβ in the presence of HSA and found that HSA retards fibril growth in a concentration-dependent manner and reduces the amount of fibrils formed which is in agreement with our results.[40] However, in their study, there is no evidence of ThT interference due to HSA, even at 10 μM quantities, whereas ThT interference already starts around 3 μM in our experiments as seen in Figure 5a.

Elevated levels of ThT fluorescence are also observed when negatively charged polystyrene nanoparticles are used in studies of the effect on FAβ42 fibril formation. Figure 5d shows the progressive increase of the ThT signals during the reaction time course with increasing nanoparticle concentrations. Note that the aggregation curves still show a sigmoidal-like shape at lower nanoparticle concentrations. However, the initial intensities are increased compared to the control IR680-FAβ42 ThT intensity when no nanoparticle is present. Figure 5e shows the results of the filter-trap assay for fibril formation of IR680-FAβ42 at two nanoparticle concentrations. At low concentration of nanoparticles, IR680-FAβ42 fibril formation seems to be accelerated compared to that in the control without nanoparticles. The effect is reversed at high nanoparticle concentration. However, the plateau intensities of samples with two different nanoparticle concentrations do not change when the concentration of nanoparticle is increased. When data sets are normalized to the highest intensity value in all three data sets of the nanoparticle experiment, final fluorescence intensity values of the fibrils trapped on the membrane in the presence of two different nanoparticle concentrations are the same and twice that of IR680-FAβ42 without any particles. To make sure that fibrils are formed in the presence of different nanoparticle concentrations, TEM images were taken at the end of the experiment. Figure 5f shows the aggregates form in the presence of nanoparticles, indicating that our findings are indeed due to fibril formation. It is not clear in Figure 5f whether nanoparticles are associated along the fibrils or not because the negative-staining procedure is based on force drying the reaction mixture; therefore, the association of elements is inevitable.

Effects of nanoparticles on amyloid fibril formation and indirect implications on AD are very much of interest in the field. Nanoparticles are entities that are smaller than micron size, made from a widespread range of materials. Naturally existing nanoparticles aside, industrialization caused different paths for the passive uptake of nanoparticles into the human body, and a vast majority of nanoparticles are actively taken through many consumer products. Moreover, several drug delivery systems are based on nanoparticles as cargo holders; hence, it becomes impossible to avoid the exposure to good and bad nanoparticles. Variations of these systems arise from the types of nanoparticles, from bare to modified surfaces[41−43] with tuned hydrophobicities,[12] and were studied extensively. Most research conducted to date has shown that nanoparticles inhibit fibril formation,[12,42−45] with few exceptions of acceleration and dual behaviors, in which both acceleration and retardation were seen depending on the concentration of the nanoparticles added.[41,46,47] Vacha and co-workers found that the ThT signal becomes distorted at high concentrations of 26 nm polystyrene nanoparticles with carboxyl surface modification[46] and that they could not perform kinetic studies at the high nanoparticle concentrations mentioned because of the ThT intensity being masked. This finding is confirmed here as seen in Figure 5d,

DOI: 10.1021/acschemneuro.5b00104
ACS Chem. Neurosci. 2015, 6, 1436−1444

where the initial ThT signal increases with increasing concentration of carboxyl modified 49 nm nanoparticles, making data analyses unreliable. With the filter-trap assay, a dual behavior (acceleration at low nanoparticle concentrations and retardation at high nanoparticle concentration) is observed, and the equilibrium fluorophore intensity is 2-fold higher than that of the IR680-FAβ42. Our results are in line with the literature where nanoparticle concentration dependent dual behaviors of fibril formation $t_{1/2}$s are observed with different polystyrene particles.[46,47] Moreover, these findings suggest a difference in the amount of fibrils formed at equilibrium, regardless of the kinetic deviations in fibril formation.

Current Limitations and Future Outlook. A major limitation of the method proposed is its semicontinuous nature. This limits the accuracy and precision in data analysis because less number of time points are recorded compared to that in continuous assays. The filter-trap assay is here used to monitor a kinetic process; thus, possible perturbation of the kinetics by separation of the components from the solution needs to be ruled out by comparing the method to other kinetic methods. In our case, complementary traces of both the retentate and the flow through reaction reveal the same trends. Additionally, when compared to ThT experiments, similar traces are observed. The ThT assay has been proven to be a reliable kinetic method by Cukalevski et al. with delicate experiments of adding ThT at different stages of fibril formation, yet obtaining the same kinetic parameters, which are further validated by kinetic experiments monitored by CD spectroscopy.[48] However, it is important to highlight that the ThT assay and the filter-trap assay report on different features (β-sheets and size discrimination, respectively), and deviations in the kinetic parameters obtained by the two methods might provide additional mechanistic insights.

Further developments of the method can include automation, e.g., at the sample collection and/or the filtration steps that would make it much easier to apply. Moreover, the method can be customized to fit the requirements of the amyloid system of choice by changing the membrane material, cut off size, peptide labeling strategy, and the fluorophore. Our method can also be used in FRET studies of peptides employing two different fluorescent labels.

METHODS

Materials. All chemicals were of the highest purity available. Alexa Fluor 488 dye was purchased from Life Technologies and IRDye 680RD infrared dye was purchased from LI-COR. Fatty acid free albumin from human serum (HSA) of purity ≥96% was purchased from Sigma, dissolved in 20 mM sodium phosphate buffer and 200 μM EDTA at pH 8, and filtered through a 0.2 μm cellulose acetate filter to remove contaminants and aggregates. The HSA concentration was spectrophotometrically determined at 280 nm using 35495 $M^{-1}cm^{-1}$ as the extinction coefficient.[49] Polystyrene nanoparticles of 49 nm nominal size with carboxyl surface modification were purchased from Polysciences, Inc. Particles were dialyzed against water for 1 week to remove stabilizers.

Protein Purification. Aβ(M1−42), was expressed in *Escherichia coli* from a synthetic gene and purified as described previously.[50] Briefly, the purification procedure involved sonication of *E. coli* cells, dissolution of inclusion bodies in 8 M urea, anion-exchange in batch mode on DEAE cellulose resin, centrifugation through a 30 kDa molecular weight cutoff (MWCO) filter, and finally concentration using a 5 kDa MWCO filter. The purified peptide was frozen in 1 mL aliquots. A cysteine containing variant of Aβ42, Aβ(MC1−42), was expressed and purified as described above with the only exception of the addition of 0.01 mM DTT throughout the cell breaking process.

Immediately before each experiment, freeze-dried Aβ42 samples were dissolved in 6 M guanidinium chloride and subjected to gel filtration and buffer exchange on a Superdex 75 10/300 GL column (GE Healthcare) in 20 mM sodium phosphate buffer and 200 μM EDTA at pH 8. The monomer fraction was collected and kept on ice. The monomer concentration was calculated from integration of the monomer peak in the chromatogram using an extinction coefficient at 280 nm of 1440 $M^{-1}cm^{-1}$.[50]

Labeling of Aβ42. Aβ(MC1−42) was freeze-dried prior to each labeling process, and monomers were quantified as described above except for using a buffer without EDTA and with 100 μM DTT as reducing agent. Alexa Fluor 488 dye and IRDye 680RD infrared dye were each dissolved in water at concentrations between 2 and 400 times that of the Aβ(MC1−42) monomers. Dye solution was added to the freshly collected monomers dropwise with invertion after each drop to achieve uniform mixing. The dye−monomer solution was kept at room temperature for 2 h or on ice overnight for labeling. After incubation, another size exclusion step was performed to eliminate the aggregated species and free dye. The concentration of the labeled peptide was estimated by using the absorbance values for each dye at λ_{500} for Alexa Fluor 488 dye and λ_{692} for IRDye 680RD infrared dye. Extinction coefficients at the specified wavelengths are 71000 $M^{-1}\cdot cm^{-1}$ and 165000 $M^{-1}\cdot cm^{-1}$, respectively.[51]

Thioflavin T Kinetic Assay. The freshly purified monomer of unlabeled Aβ42 was diluted to 2.5 to 6 μM (depending on the experiment) in 20 mM sodium phosphate buffer and 200 μM EDTA at pH 8. This stock solution was mixed in appropriate ratios with a stock solution of the equal concentration of labeled Aβ42 monomer. This mixture of unlabeled and fluorophore labeled peptide is referred to here as FAβ42, and the type of fluorophores is specified with prefixes A488 or IR680 for Alexa Fluor 488 dye and IRDye 680RD infrared dye, respectively. Control samples of unlabeled Aβ42 were also prepared at equal total concentration to FAβ42 monomers to determine the possible effect of labeling on fibrillation. ThT (CalbioChem) was added to FAβ42 and to control unlabeled Aβ42 from a stock of 1.4 mM in working buffer, to a final concentration of 14 μM, and samples were aliquoted into a 96-well half-area plate of black polystyrene with a clear bottom and nonbinding surface (Corning 3881) on ice. ThT fluorescence intensity was measured continuously at 37 °C in a plate reader (Fluostar Omega or Fluostar Optima, BMG Labtech, Offenburg, Germany) until a plateau was reached (excitation filter 440 nm and emission filter 480 nm).

Filter-Trap Assay. Samples for the filter-trap assay were prepared in the same way as that for the ThT assay omitting ThT from the mixture. During the course of fibrillation, FAβ42 samples (100 μL) were collected from the 96-well plate according to the progression of ThT containing FAβ42 controls and placed on an AcroPrep 96-well filter plate embedded with a Versatile GH Polypro membrane (hereafter will be referred as GHP) (Pall Life Sciences, Ann Arbor, MI) with each time point having 2 or 3 replicates. Before loading the GHP membrane with time point samples, all wells of the GHP membrane plate were washed with working buffer. MultiScreen$_{HTS}$ vacuum (Millipore) manifold loading was done as follows: inside the manifold housing, first a 96-well black polystyrene transparent bottom plate was placed to collect the flow through, with the GHP membrane plate placed on top. The manifold was tightened, and vacuum applied for about 10 s. The fluorescence intensity of the retentate on the GHP membrane plate and the flow through in polystyrene plate was measured in a plate reader (Fluostar Omega or Fluostar Optima or ClarioStar BMG Labtech, Offenburg, Germany) with filters (Alexa Fluor 488 dye, λ_{ex} 485 nm and λ_{em} 520 nm; IRDye 680RD infrared dye, λ_{ex} 660 nm and λ_{em} 710 nm). The gain of the instrument was optimized for each plate to yield the best intensity values for each fluorophore. Other filter membrane plates used in this study to test the signal to blank ratio were FiltrEX 0.2 μM PVDF membrane (Corning 3505) and MultiScreen$_{HTS}$ GV filter plate, 0.22 μm (Millipore), BioTrace NT (Pall), Supor PES (Pall), Bio-Inert (Pall), glass fiber (Corning), and mixed cellulose (Millipore).

To study the effect of HSA on amyloid fibril formation, stocks of A488-FAβ42 monomers and HSA were prepared at twice the final

DOI: 10.1021/acschemneuro.5b00104
ACS Chem. Neurosci. 2015, 6, 1436−1444

concentration and mixed in equal volumes. The samples were incubated, frozen at different time points, and filtered as described previously. For nanoparticle experiments, 10 times the final concentration stock of nanoparticles and 1.1 times the final concentration stock of IR680-FAβ42 were mixed in a 1:9 volume ratio. Samples were incubated as described above, and aliquots of 100 μL for each time point were immediately filtered to prevent freezing-induced nanoparticle gel formation, as pointed out in instructions from the manufacturer.

Transmission Electron Microscopy. Eight microliters of sample that had formed fibrils according to the filter-trap assay was applied to a 300 mesh carbon-coated Formvar grid (Electron Microscopy Sciences, Hatfield, PA) for 3 min, blotted with filter paper, stained with 1.5% uranyl acetate (Merck) (w/v) in water for 30 s, blotted with filter paper again, and washed with water followed by another blotting step. The samples were analyzed with a Philips CM120 BioTWIN cryo TEM at 6200× and 31000× magnifications.

■ ASSOCIATED CONTENT

Supporting Information

TEM images of flow through fractions and A488-FAβ fibrils in the presence of varying concentrations of HSA, tables containing sequences of Aβ(M1−42) and Aβ(MC1−42), and the sample to blank values of different plates tested are included. The Supporting Information is available free of charge on the ACS Publications website at DOI: 10.1021/acschemneuro.5b00104.

■ AUTHOR INFORMATION

Corresponding Author

*E-mail: Irem.Nasir@biochemistry.lu.se.

Author Contributions

I.N., S.L., and C.C.-L. planned and performed the experiments. I.N., S.L., and C.C.-L. analyzed the data and wrote the manuscript.

Funding

We acknowledge funding from following resources: Swedish Research Council (VR) (to C.C.-L. and S.L.), the Royal Physiographic Society and the Crafoord Foundation (to C.C.-L.), and European Research Council Advanced Grant (to S.L.).

Notes

The authors declare no competing financial interest.

■ ACKNOWLEDGMENTS

We gratefully acknowledge Jannette Carey at the Chemistry Department, Princeton University for valuable input on the manuscript. We also thank Gunnel Karlsson at the Biomicroscopy Unit, Polymer and Materials Chemistry, Chemical Centre, Lund University for the assistance with transmission electron microscopy.

■ REFERENCES

(1) Ballard, C., Gauthier, S., Corbett, A., Brayne, C., Aarsland, D., and Jones, E. (2011) Alzheimer's disease. *Lancet 377*, 1019−1031.

(2) Chiti, F., and Dobson, C. M. (2006) Protein misfolding, functional amyloid, and human disease. *Annu. Rev. Biochem.*, 333−366.

(3) Finder, V. H. (2010) Alzheimer's disease: A general introduction and pathomechanism. *J. Alzheimer's Dis. 22*, S5−S19.

(4) Naslund, J., Schierhorn, A., Hellman, U., Lannfelt, L., Roses, A. D., Tjernberg, L. O., Silberring, J., Gandy, S. E., Winblad, B., Greengard, P., Nordstedt, C., and Terenius, L. (1994) Relative abundance of alzheimer a-beta amyloid peptide variants in alzheimer-disease and normal aging. *Proc. Natl. Acad. Sci. U.S.A. 91*, 8378−8382.

(5) Walsh, D. M., Hartley, D. M., Kusumoto, Y., Fezoui, Y., Condron, M. M., Lomakin, A., Benedek, G. B., Selkoe, D. J., and Teplow, D. B. (1999) Amyloid beta-protein fibrillogenesis - structure and biological activity of protofibrillar intermediates. *J. Biol. Chem. 274*, 25945−25952.

(6) Hardy, J. A., and Higgins, G. A. (1992) Alzheimers disease - the amyloid cascade hypothesis. *Science 256*, 184−185.

(7) Bateman, D. A., McLaurin, J., and Chakrabartty, A. (2007) Requirement of aggregation propensity of alzheimer amyloid peptides for neuronal cell surface binding, *BMC Neurosci. 8*.

(8) Cohen, S. I. A., Vendruscolo, M., Dobson, C. M., and Knowles, T. P. J. (2012) From macroscopic measurements to microscopic mechanisms of protein aggregation. *J. Mol. Biol. 421*, 160−171.

(9) Assarsson, A., Hellstrand, E., Cabaleiro-Lago, C., and Linse, S. (2014) Charge dependent retardation of amyloid beta aggregation by hydrophilic proteins. *ACS Chem. Neurosci. 5*, 266−274.

(10) Assarsson, A., Linse, S., and Cabaleiro-Lago, C. (2014) Effects of polyamino acids and polyelectrolytes on amyloid beta fibril formation. *Langmuir 30*, 8812−8818.

(11) Cabaleiro-Lago, C., Lynch, I., Dawson, K. A., and Linse, S. (2010) Inhibition of iapp and iapp((20−29)) fibrillation by polymeric nanoparticles. *Langmuir 26*, 3453−3461.

(12) Cabaleiro-Lago, C., Quinlan-Pluck, F., Lynch, I., Lindman, S., Minogue, A. M., Thulin, E., Walsh, D. M., Dawson, K. A., and Linse, S. (2008) Inhibition of amyloid beta protein fibrillation by polymeric nanoparticles. *J. Am. Chem. Soc. 130*, 15437−15443.

(13) Hard, T., and Lendel, C. (2012) Inhibition of amyloid formation. *J. Mol. Biol. 421*, 441−465.

(14) Rozga, M., Kloniecki, M., Jablonowska, A., Dandlez, M., and Bal, W. (2007) The binding constant for amyloid a beta 40 peptide interaction with human serum albumin. *Biochem. Biophys. Res. Commun. 364*, 714−718.

(15) Shammas, S. L., Waudby, C. A., Wang, S., Buell, A. K., Knowles, T. P. J., Ecroyd, H., Welland, M. E., Carver, J. A., Dobson, C. M., and Meehan, S. (2011) Binding of the molecular chaperone alpha b-Crystallin to a beta amyloid fibrils inhibits fibril elongation. *Biophys. J. 101*, 1681−1689.

(16) Hughes, E., Burke, R. M., and Doig, A. J. (2000) Inhibition of toxicity in the beta-amyloid peptide fragment beta-(25−35) using n-methylated derivatives - a general strategy to prevent amyloid formation. *J. Biol. Chem. 275*, 25109−25115.

(17) LeVine, H. (1999) Quantification of beta-sheet amyloid fibril structures with thioflavin t. *Methods Enzymol. 309*, 274−284.

(18) Bruggink, K. A., Mueller, M., Kuiperij, H. B., and Verbeek, M. M. (2012) Methods for analysis of amyloid-beta aggregates. *J. Alzheimer's Dis. 28*, 735−758.

(19) Hellstrand, E., Boland, B., Walsh, D. M., and Linse, S. (2010) Amyloid beta-protein aggregation produces highly reproducible kinetic data and occurs by a two-phase process. *ACS Chem. Neurosci. 1*, 13−18.

(20) Noormai, A., Primar, K., Tougu, V., and Palumaa, P. (2012) Interference of low-molecular substances with the thioflavin-t fluorescence assay of amyloid fibrils. *J. Pept. Sci. 18*, 59−64.

(21) Necula, M., Kayed, R., Milton, S., and Glabe, C. G. (2007) Small molecule inhibitors of aggregation indicate that amyloid beta oligomerization and fibrillization pathways are independent and distinct. *J. Biol. Chem. 282*, 10311−10324.

(22) Jameson, L. P., Smith, N. W., and Dzyuba, S. V. (2012) Dye-binding assays for evaluation of the effects of small molecule inhibitors on amyloid (a beta) self-assembly. *ACS Chem. Neurosci. 3*, 807−819.

(23) Winklhofer, K. F., Hartl, F. U., and Tatzelt, J. (2001) A sensitive filter retention assay for the detection of prpsc and the screening of anti-prion compounds. *FEBS Lett. 503*, 41−45.

(24) Wanker, E. E., Scherzinger, E., Heiser, V., Sittler, A., Eickhoff, H., and Lehrach, H. (1999) Membrane filter assay for detection of amyloid-like polyglutamine-containing protein aggregates. *Methods Enzymol. 309*, 375−386.

(25) Chang, E., and Kuret, J. (2008) Detection and quantification of tau aggregation using a membrane filter assay. *Anal. Biochem. 373*, 330−336.

DOI: 10.1021/acschemneuro.5b00104
ACS Chem. Neurosci. 2015, 6, 1436−1444

(26) Boye-Harnasch, M., and Cullin, C. (2006) A novel in vitro filter trap assay identifies tannic acid as an amyloid aggregation inducer for het-s. *J. Biotechnol. 125*, 222−230.
(27) Jungbauer, L. M., Yu, C., Laxton, K. J., and LaDu, M. J. (2009) Preparation of fluorescently-labeled amyloid-beta peptide assemblies: The effect of fluorophore conjugation on structure and function. *J. Mol. Recognit. 22*, 403−413.
(28) Petkova, A. T., Ishii, Y., Balbach, J. J., Antzutkin, O. N., Leapman, R. D., Delaglio, F., and Tycko, R. (2002) A structural model for alzheimer's beta-amyloid fibrils based on experimental constraints from solid state nmr. *Proc. Natl. Acad. Sci. U.S.A. 99*, 16742−16747.
(29) Cohen, S. I. A., Arosio, P., Presto, J., Kurudenkandy, F. R., Biverstal, H., Dolfe, L., Dunning, C., Yang, X., Frohm, B., Vendruscolo, M., Johansson, J., Dobson, C. M., Fisahn, A., Knowles, T. P. J., and Linse, S. (2015) A molecular chaperone breaks the catalytic cycle that generates toxic abeta oligomers. *Nat. Struct. Mol. Biol. 22*, 207−213.
(30) Anderson, V. L., and Webb, W. W. (2011) Transmission electron microscopy characterization of fluorescently labelled amyloid beta 1−40 and alpha-synuclein aggregates, *BMC Biotechnol. 11*.
(31) Cohen, S. I. A., Linse, S., Luheshi, L. M., Hellstrand, E., White, D. A., Rajah, L., Otzen, D. E., Vendruscolo, M., Dobson, C. M., and Knowles, T. P. J. (2013) Proliferation of amyloid-beta 42 aggregates occurs through a secondary nucleation mechanism. *Proc. Natl. Acad. Sci. U.S.A. 110*, 9758−9763.
(32) He, X. M., and Carter, D. C. (1992) Atomic-structure and chemistry of human serum-albumin. *Nature 358*, 209−215.
(33) Llewellyn, D. J., Langa, K. M., Friedland, R. P., and Lang, I. A. (2010) Serum albumin concentration and cognitive impairment. *Curr. Alzheimer's Res. 7*, 91−96.
(34) Kuo, Y. M., Emmerling, M. R., Lampert, H. C., Hempelman, S. R., Kokjohn, T. A., Woods, A. S., Cotter, R. J., and Roher, A. E. (1999) High levels of circulating a beta 42 are sequestered by plasma proteins in alzheimer's disease. *Biochem. Biophys. Res. Commun. 257*, 787−791.
(35) Sen, P., Fatima, S., Ahmad, B., and Khan, R. H. (2009) Interactions of thioflavin t with serum albumins: Spectroscopic analyses. *Spectrochim. Acta, Part A 74*, 94−99.
(36) Taboada, P., Barbosa, S., Castro, E., and Mosquera, V. (2006) Amyloid fibril formation and other aggregate species formed by human serum albumin association. *J. Phys. Chem. B 110*, 20733−20736.
(37) Milojevic, J., Raditsis, A., and Melacini, G. (2009) Human serum albumin inhibits a beta fibrillization through a "monomer-competitor" mechanism. *Biophys. J. 97*, 2585−2594.
(38) Milojevic, J., and Melacini, G. (2011) Stoichiometry and affinity of the human serum albumin-alzheimer's a beta peptide interactions. *Biophys. J. 100*, 183−192.
(39) Milojevic, J., Esposito, V., Das, R., and Melacini, G. (2007) Understanding the molecular basis for the inhibition of the alzheimer's a beta-peptide oligomerization by human serum albumin using saturation transfer difference and off-resonance relaxation nmr spectroscopy. *J. Am. Chem. Soc. 129*, 4282−4290.
(40) Stanyon, H. F., and Viles, J. H. (2012) Human serum albumin can regulate amyloid-beta peptide fiber growth in the brain interstitium implications for alzheimer disease. *J. Biol. Chem. 287*, 28163−28168.
(41) Wu, W.-h., Sun, X., Yu, Y.-p., Hu, J., Zhao, L., Liu, Q., Zhao, Y.-f., and Li, Y.-m. (2008) Tio2 nanoparticles promote beta-amyloid fibrillation in vitro. *Biochem. Biophys. Res. Commun. 373*, 315−318.
(42) Rocha, S., Thueneman, A. F., Pereira, M. d. C., Coelho, M., Moehwald, H., and Brezesinski, G. (2008) Influence of fluorinated and hydrogenated nanoparticles on the structure and fibrillogenesis of amyloid beta-peptide. *Biophys. Chem. 137*, 35−42.
(43) Araya, E., Olmedo, I., Bastus, N. G., Guerrero, S., Puntes, V. F., Giralt, E., and Kogan, M. J. (2008) Gold nanoparticles and microwave irradiation inhibit beta-amyloid amyloidogenesis. *Nanoscale Res. Lett. 3*, 435−443.
(44) Yoo, S. I., Yang, M., Brender, J. R., Subramanian, V., Sun, K., Joo, N. E., Jeong, S.-H., Ramamoorthy, A., and Kotov, N. A. (2011) Inhibition of amyloid peptide fibrillation by inorganic nanoparticles: Functional similarities with proteins. *Angew. Chem., Int. Ed. 50*, 5110−5115.
(45) Liao, Y.-H., Chang, Y.-J., Yoshiike, Y., Chang, Y.-C., and Chen, Y.-R. (2012) Negatively charged gold nanoparticles inhibit alzheimer's amyloid-beta fibrillization, induce fibril dissociation, and mitigate neurotoxicity. *Small 8*, 3631−3639.
(46) Vacha, R., Linse, S., and Lund, M. (2014) Surface effects on aggregation kinetics of amyloidogenic peptides. *J. Am. Chem. Soc. 136*, 11776−11782.
(47) Cabaleiro-Lago, C., Quinlan-Pluck, F., Lynch, I., Dawson, K. A., and Linse, S. (2010) Dual effect of amino modified polystyrene nanoparticles on amyloid beta protein fibrillation. *ACS Chem. Neurosci. 1*, 279−287.
(48) Cukalevski, R., Boland, B., Frohm, B., Thulin, E., Walsh, D., and Linse, S. (2012) Role of aromatic side chains in amyloid beta-protein aggregation. *ACS Chem. Neurosci. 3*, 1008−1016.
(49) Pace, C. N., Vajdos, F., Fee, L., Grimsley, G., and Gray, T. (1995) How to measure and predict the molar absorption-coefficient of a protein. *Protein Sci. 4*, 2411−2423.
(50) Walsh, D. M., Thulin, E., Minogue, A. M., Gustavsson, N., Pang, E., Teplow, D. B., and Linse, S. (2009) A facile method for expression and purification of the alzheimer's disease-associated amyloid beta-peptide. *FEBS J. 276*, 1266−1281.
(51) Rusinova, E., Tretyachenko-Ladokhina, V., Vele, O. E., Senear, D. F., and Ross, J. B. A. (2002) Alexa and oregon green dyes as fluorescence anisotropy probes for measuring protein-protein and protein-nucleic acid interactions. *Anal. Biochem. 308*, 18−25.

DOI: 10.1021/acschemneuro.5b00104
ACS Chem. Neurosci. 2015, 6, 1436−1444